INTERNATIONAL JOURNAL FOR NUMERICAL METHODS IN FLUIDS, VOL. 12, 809–823 (1991)

AN AXISYMMETRIC MODEL OF SEPARATED FLOW ABOUT A SPHERE USING DISCRETE VORTICES

D. K. LEE*

Department of Naval Architecture and Ocean Engineering, University of Ulsan, Ulsan, Korea

AND

M. J. DOWNIE AND P. BETTESS

Department of Marine Technology, University of Newcastle upon Tyne, Newcastle upon Tyne, U.K.

SUMMARY

A procedure for the calculation of the starting flow around a sphere in a uniform stream is presented. The flow field is simulated by a flow of ideal fluid with embedded vorticity. With the assumption that the flow remains symmetric, the vorticity field is approximated by a number of discrete circular line vortices. The image vortices to satisfy the boundary condition for the normal component of velocity on the surface of the sphere are determined by Butler's sphere theorem. The Stokes streamfunction is used for the field description. The motion of vortices is tracked by the vortex-in-cell method, the cells being formed by square grids.

KEY WORDS Axisymmetric flow Sphere Vortices Discrete vortices Cloud in cell

1. INTRODUCTION

There are many engineering problems involving the flow of a fluid past a body which in the past have been impossible to treat by the solution of the Navier–Stokes equations, largely owing to limitations on computing resources. Even with today's supercomputers, this is still the case with some problems and, at least in the immediate future, will remain so. Alternative strategies have, of necessity, evolved and one of these is to model the problem by the use of singularities embedded in a potential flow field. Examples of the success of this strategy may readily be found in the surface vorticity methods developed in the fields of aerofoil and propellor theory. Of course, this approach also has its limitations. By its very nature it is unable to predict frictional drag, and the models have no Reynolds number dependence. However, if not pushed beyond their limitations, models based on this approach can produce results in very good agreement with those obtained experimentally. An early notable example is the prediction of the lift force on an aerofoil.

More recently, two-dimensional incompressible separated flows about bluff bodies at high Reynolds numbers have been treated on a similar basis. In this case the flow is time-dependent and vorticity is continuously fed into the wake. In early models of this nature, based on the discrete vortex method and developed from the 1960s onwards, the Reynolds number was not

* Visiting Professor at the University of Newcastle upon Tyne.

0271–2091/91/090809–15$07.50

Received September 1989
Revised October 1990

defined explicitly but was assumed to be high enough for the viscous effects to be negligible other than in the original generation of vorticity at the surface of the body. The impetus for these models arose from the observation that interacting shear layers computed by Abernathy and Kronauer,[1] for example, closely resembled the physical flows found in the wake of bluff bodies.[2] The most encouraging aspects of the early models were qualitative rather than quantitative. However, they evolved into the powerful methods in use today. In contemporary models the vorticity transport equation is solved in its entirety using hybrid techniques in which the convection part is solved by the discrete vortex method and the viscous diffusion by random walks or difference schemes. Comprehensive reviews of these methods have been published by Maull[3] and Sarpkaya.[4] Suffice it to say that convincing results have been obtained for a number of varied and difficult time-dependent flows using these methods.

The success achieved with two-dimensional models has inevitably led to an interest in their extension to three dimensions. Leonard,[5] for instance, has investigated the flow about a sphere using closed vortex filaments. Kamemoto *et al.*[6] have modelled the axisymmetric flow obtained with a circular disc with a concentric hole in it and subjected to a uniform stream, by using vortex rings. The present study was inspired by similar considerations and is viewed as a preliminary stage in a long-term project ultimately aimed at achieving a model for three-dimensional flow about an arbitrary body.

The study is concerned with modelling axisymmetric separated flow about a sphere. As with the discrete vortex method, the Reynolds number is not explicitly defined and, similarly, the model is appropriate to high-Reynolds-number regimes. Its most obvious application is to the starting flow about a sphere in a uniform stream. However, it is envisaged that it might also be appropriate to the near wake of more fully developed flows. Various experiments have been carried out on the flow about spheres and they all show that at high Reynolds numbers, after an initial starting flow, the wake becomes unstable and loses all semblance of symmetry. There is a certain amount of disagreement about the Reynolds number range at which this happens. It is no doubt highly sensitive to the exact conditions under which the experiment is carried out, and affected, amongst other factors, by how the sphere is supported. Flow visualization experiments[7, 8] demonstrate that it is possible to obtain axisymmetric conditions in the near wake up to moderately high Reynolds numbers of the order of 10^4, see for example Figure 1.[8] In addition to this, the discrete vortex method applied to two-dimensional flow about a circular cylinder was found to be able to produce results appropriate to the subcritical regime; that is, at lower Reynolds numbers than might have been expected from the assumptions on which the model is based. The study was undertaken partly with the object of modelling the starting flows about spheres, partly to investigate the applicability of the model to the near wake of more fully developed flows and partly in the spirit of a numerical experiment aimed at gaining experience in the modelling of axisymmetric separated flows.

2. THE STREAMFUNCTION AND THE VELOCITY

The wake, being a rotational flow, may be approximated by a distribution of discrete vortices, all of which are in fact circular line vortices because of the axisymmetry of the flow. The Stokes streamfunction can be defined for each of these and is, in a cylindrical co-ordinate system, given by[9]

$$\psi(x, a)=\frac{\sqrt{(a\rho)}}{2\pi}\,\Gamma\left[\left(\frac{2}{\kappa}-\kappa\right)K(\kappa)-\frac{2}{\kappa}E(\kappa)\right], \tag{1}$$

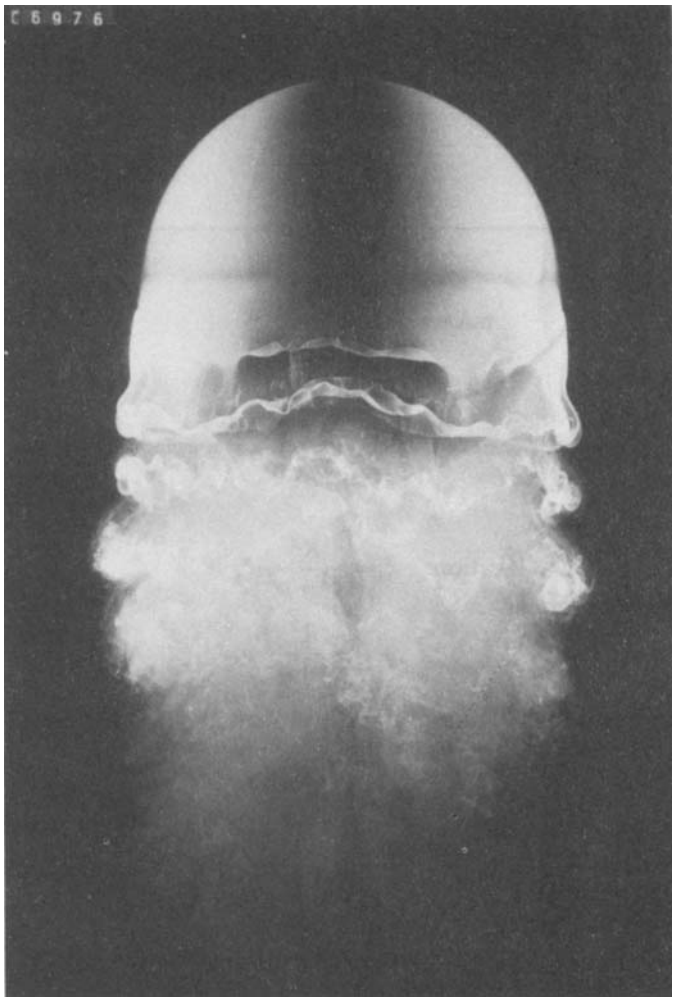

Figure 1. Flow visualization photograph, Werlé[8]

where

$$\kappa(x, a; \xi, \rho) = \left(\frac{4a\rho}{(x-\xi)^2 + (a+\rho)^2} \right)^{1/2}. \tag{2}$$

Suppose a sphere of radius R is put within a uniform steady stream of speed U in the positive x-direction so that its centre coincides with the origin of the cylindrical co-ordinate system (Figure 2). If there is an axisymmetric circular line vortex of strength Γ at a point (ξ, ρ) in the xa-plane, an axisymmetric image circular line vortex is required to satisfy the zero-normal-velocity boundary condition on the surface of the sphere. The problem of an image within a sphere was dealt with by Lewis,[10] this work being eventually surpassed by Butler's sphere theorem.[11] According to these works, the image vortex is specified by

$$\text{strength:} \quad \Gamma_i = -\frac{(\xi^2 + \rho^2)^{1/2}}{R} \Gamma, \tag{3}$$

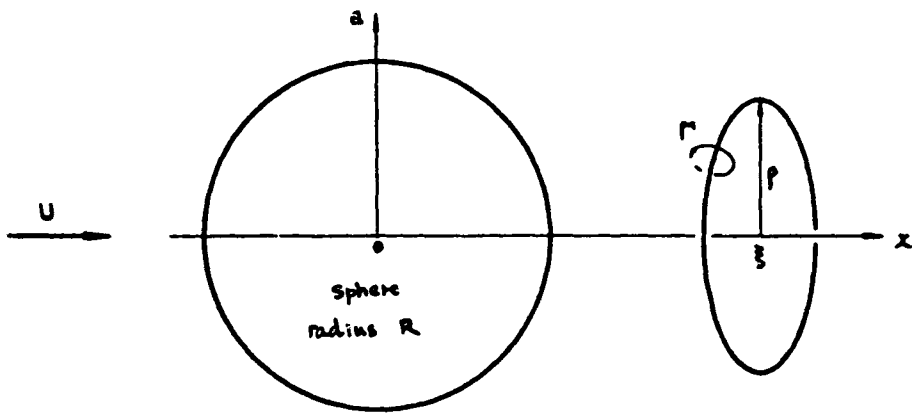

Figure 2. Sphere and circular line vortex in a uniform stream

$$\text{location:} \quad \xi_i = \frac{R^2}{\xi^2+\rho^2}\,\xi, \tag{4a}$$

$$\rho_i = \frac{R^2}{\xi^2+\rho^2}\,\rho. \tag{4b}$$

The resulting streamfunction, made up of the free stream about the sphere, N external discrete vortices and the same number of image vortices, is expressed by

$$\psi(x,a) = \frac{1}{2}Ua^2\left(1-\frac{R^3}{(x^2+a^2)^{3/2}}\right) + \sum_{k=1}^{N}\sqrt{\left(\frac{a\rho_k}{2\pi}\right)}\Gamma_k\left[\left(\frac{2}{\kappa_k}-\kappa_k\right)K(\kappa_k)-\frac{2}{\kappa_k}E(\kappa_k)\right]$$
$$+\sum_{k=1}^{N}\sqrt{\left(\frac{a\rho_{ik}}{2\pi}\right)}\Gamma_{ik}\left[\left(\frac{2}{\kappa_{ik}}-\kappa_{ik}\right)K(\kappa_{ik})-\frac{2}{\kappa_{ik}}E(\kappa_{ik})\right], \tag{5}$$

where

$$\kappa_k = \kappa(x, a; \xi_k, \rho_k), \tag{6a}$$

$$\kappa_{ik} = \kappa(x, a; \xi_{ik}, \rho_{ik}). \tag{6b}$$

The non-dimensional co-ordinates, velocity and time may be defined by

$$\text{co-ordinates:} \quad x' = x/R \quad \text{and} \quad a' = a/R, \tag{7a}$$

$$\text{velocity:} \quad u' = u/U \quad \text{and} \quad v' = v/U, \tag{7b}$$

$$\text{time:} \quad t' = t/(R/U). \tag{7c}$$

The velocity components are then expressed in terms of these non-dimensional variables (with the primes omitted) by the following:

$$u(x,a) = 1+\frac{a^2-2x^2}{2r^5}+\sum_{k=1}^{N}\left[\Gamma_k G_x(x,a;\xi_k,\rho_k)+\Gamma_{ik}G_x(x,a;\xi_{ik},\rho_{ik})\right], \tag{8a}$$

$$v(x,a) = \frac{-3ax}{2r^5}+\sum_{k=1}^{N}\left[\Gamma_k G_a(x,a;\xi_k,\rho_k)+\Gamma_{ik}G_a(x,a;\xi_{ik},\rho_{ik})\right]. \tag{8b}$$

where

$$r=(x^2+a^2)^{1/2}, \tag{9}$$

$$G_x(x, a; \xi, \rho)=\frac{\kappa}{4\pi\sqrt{(a\rho)}}\left[K(\kappa)-\frac{1}{2}\left(1+\frac{1-(\rho/a)\kappa^2}{1-\kappa^2}\right)E(\kappa)\right], \tag{10a}$$

$$G_a(x, a; \xi, \rho)=\frac{-(x-\xi)}{4\pi a\sqrt{(a\rho)}}\kappa\left[K(\kappa)-\frac{1}{2}\left(1+\frac{1}{1-\kappa^2}\right)E(\kappa)\right], \tag{10b}$$

$$\kappa(x, a; \xi, \rho)=\left(\frac{4a\rho}{(x-\xi)^2+(a+\rho)^2}\right)^{1/2}. \tag{11}$$

3. THE SELF-INDUCED VELOCITY

Unlike the straight line vortex presumed in two-dimensional problems, a mathematically idealized line vortex with curvature placed in an ideal fluid acquires a self-convecting velocity in a locally binormal direction and of logarithmically infinite magnitude. However, if the vortex has a finite core, it also experiences a finite self-induced velocity. It is therefore necessary to model a core whose nature will depend on how the diffusive effect of viscosity is accounted for and how the vorticity is distributed within it. If the diffusion effect is neglected and the vorticity is assumed to be constant within the core, the Kelvin–Lamb formula for a circular line vortex is obtained:

$$U_{\text{self}}=\frac{\Gamma}{4\pi\rho}\left[\log\left(\frac{8\rho}{\varepsilon}\right)-\frac{1}{4}\right]. \tag{12}$$

The core radius can still change with time if the radius of the vortex increases or decreases, according to the rule that the volume of vortex core is invariant for an incompressible fluid.[9] Therefore the subsequent self-induced velocity may be expressed by

$$U_{\text{self}}=\frac{\Gamma}{4\pi\rho}\left\{\log\left[\frac{8}{c_c}\left(\frac{\rho}{\rho_0}\right)^{3/2}\right]-\frac{1}{4}\right\}. \tag{13}$$

The treatment of a diffused core radius can be found in Reference 12 and the logarithmic divergence of the self-induced velocity of an idealized line vortex has attracted some research interest under the topic of the 'localized induction concept'.[13]

4. MODELS OF THE VORTICITY FIELD

The vorticity in the field is concentrated in the boundary layers and the separated shear layers, and it is these areas with which the model is most fundamentally concerned. The question arises of how best to model these two elements of the flow using discrete vortices. Two possible approaches suggested themselves to the authors. The first was based on the concept of vortex sheets discretized as a series of ring vortices. In this model the boundary layer was represented by bound vortices whose strength density, which remained fairly constant apart from the area close to the separation point, was determined at every time step. The free shear layers were represented by discrete vortices introduced at the separation point at each time step and allowed to move with the flow. Their velocity was determined by the Biot–Savart law. Three aspects of this model require careful consideration. Firstly, it is necessary to determine the separation point. Secondly, measures have to be taken to prevent the sheet from becoming tangled and to delay the onset of

chaotic motion. Finally, the vortex strengths have to be determined. In this case they were taken as being equal to $\frac{1}{2}U_s^2$, which means that the separation velocity has to be determined.

At first glance the model appears an attractive one. The role played by each vortex sheet is simply related to the actual physical processes it is supposed to model, and the manner of dealing with the sheets can be clearly envisaged. Unfortunately the flow pattern predicted by the model is implausible; see Figure 3. The front of the shear layer convects downwards for a short while and then starts to roll up in a manner that is reminiscent of the starting flow about a two-dimensional cylinder. However, the rolled-up vortex sheet is not shed, but becomes increasingly convoluted and forms a confused wake, which elongates as time progresses. In fact the model provides no mechanism capable of preventing this development from occurring unless some far-fetched artifice, such as the imposition of a periodic fluctuation on the shedding rate, is introduced into it to enforce convection of the shear layer away from the sphere. Such an artifice was tried and found to work, but of course there is no justification for including it in the model.

In the second model, which is analogous to the two-dimensional vortex cloud method,[14] no distinction was made between the boundary layer and the shear layer, and the whole region of rotational flow was represented by a vorticity distribution modelled by an array of discrete vortices. At each time step the vortices were introduced at points completely surrounding the sphere and in close proximity to its surface. They were convected away by the local flow and the wake was allowed to evolve with time. The velocity calculations were carried out using the vortex-in-cell method.[14–17]

The model has a number of advantages. No assumptions have to be made with regard to the location of the separation point; the vortices are simply convected away from the sphere by the local flow. However, by the same token, the actual separation point is not well defined and there is a mixture of vortex rings of opposite sense in the immediate region of separation. The concept of a distribution of vortices, as opposed to vortex sheets, representing the vorticity field obviates the problem of sheet entanglement. The problem of the inevitable onset of chaotic motion, common to all models of this nature, is greatly delayed and diminished by the use of the vortex-in-cell velocity calculations. In the present approach the Biot–Savart law is applied at active nodes on a mesh enclosing all the discrete vortex rings in the domain of computation upon which their vorticity has been distributed. The technique is computationally more efficient than using the Biot–Savart law to calculate the velocity at each vortex ring location and allows the treatment of flows containing many more of them before their number becomes prohibitive. This approach also has the advantage that it is unnecessary to apply any explicit boundary conditions at the outer limit of the mesh. The vortex strengths were simply chosen so as to satisfy in the mean a no-slip condition on the surface of the sphere. Finally, the model provides a mechanism similar in

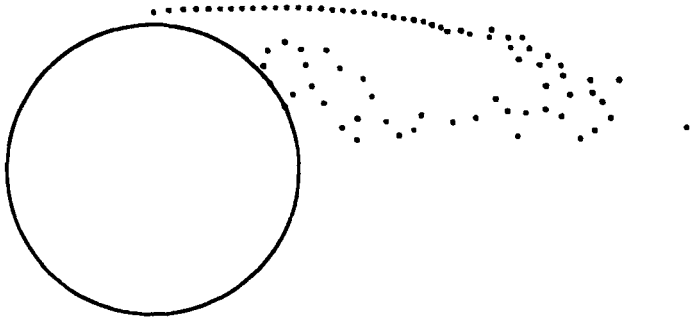

Figure 3. Predicted flow pattern, first model

nature to the 'artifice' previously described. Countervorticity generated on the rear face weakens the 'shear layer' emanating from the region of separation and enables the convection of the aggregated vorticity away from the sphere.

The second model showed some promise with regard to the evolution of the flow and the results will be discussed further after a more detailed description of the computation it involves.

5. METHOD OF COMPUTATION

The algorithm may be conveniently divided into a number of stages, each of which will be described briefly under subheadings of this section. The last seven stages, i.e. 5.5–5.11, form the basis of the part of the algorithm repeated at each time step of the calculation.

5.1. Grid formation

Rectangular polar grids are commonly used for mesh calculations about circular cylinders, and one could have been used in the present instance. However, they do have certain drawbacks. The cells become larger as the distance from the body increases, for example, although if the fine structure of the wake is to be captured in the far field, it requires the same careful treatment as the wake close to the body. More importantly, polar grids do not offer the same opportunity for taking full advantage of symmetry in constructing the velocity induction coefficient matrix (the so-called influence coefficient matrix). For these reasons square grids were used in the present computations (Figure 4). They were chosen to cover a sufficiently wide area of the downstream wake, the mesh size being 0·1 by 0·1. The choice of mesh was influenced by experience in two-dimensional calculations. It was assumed that the axisymmetric flow was analogous to this case and that the influence of factors such as 'numerical viscosity' would be similar in both instances. The mesh always encloses every discrete vortex ring in the flow.

5.2. Node-to-node influence coefficient matrices

These matrices are composed of velocity components induced at a nodal point (i, j) by the ring vortex of unit strength located at a nodal point (m, n), i.e. $G_x(x_i, a_j; x_m, a_n)$ and $G_a(x_i, a_j; x_m, a_n)$ in equations (10a) and (10b) respectively. Since G_x and G_a are functions of $x_i - x_m$ rather than of x_i

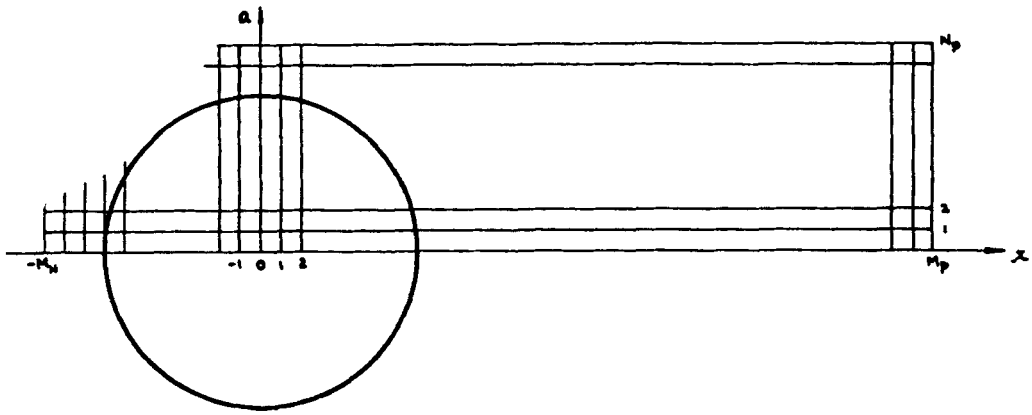

Figure 4. Grids

and x_m separately, essentially only the following values are needed:

$$G_x(x_i, a_j; 0, a_n);\ G_a(x_i, a_j; 0, a_n) \quad \text{for } i=0, 1, \ldots, M_n+M_p,\ j=0, 1, \ldots, N_p,\ n=1, 2, \ldots, N_p,$$
$$\text{except the special case of } i=0 \text{ and } j=n. \tag{14}$$

Note that the case $n=0$ corresponding to a ring vortex of zero radius is excluded.

The self-induced velocity, being dependent on the strength, the core radius and the radius of a vortex, is an intrinsic property of each vortex which cannot be treated by interpolatory procedures but must be treated individually. These matrices, therefore, are not associated with the self-induced components of velocity. From this consideration it is required that

$$G_x(0, a_n; 0, a_n)=G_a(0, a_n; 0, a_n)=0 \quad \text{for } n=1, 2, \ldots, N_p. \tag{15}$$

5.3. Calculation of the invariant factors concerned with the nascent vortices

The following parameters are determined and stored for repeated use.

(a) The co-ordinates of the nascent vortices and those of their images. In the present calculation the nascent vortices are distributed on a concentric spherical surface of radius r_{nsc} with equal angular intervals on a meridian section (Figure 5).
(b) Identification of the cell in which each of these vortices lies.
(c) The core radius coefficients. The core radius coefficient is defined as the ratio of the core radius with respect to the radius of the vortex. A nascent vortex may be taken to represent the vortex strip of width $r_{nsc}\Delta\theta$ between the midpoints of neighbouring nascent vortices on either side, as shown in Figure 6. Let this strip be held as if it were a double layer which may be deformed into a circle of the same perimeter, as suggested by Lewis.[15] Then the initial core radius coefficient is expressed by

$$c_c=\frac{\varepsilon_0}{\rho_0}=\frac{r_{nsc}\Delta\theta}{\pi\rho_0}. \tag{16}$$

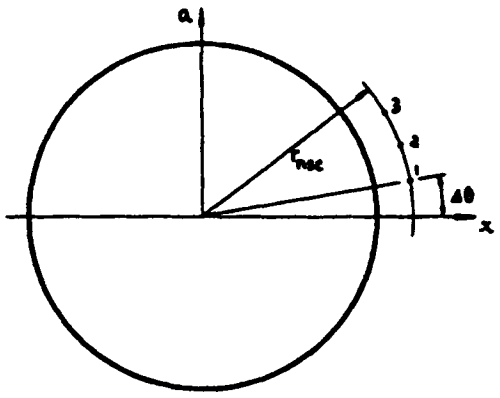

Figure 5. The nascent vortices

5.4. Calculation of the influence coefficient matrix for the tangential velocity on the surface of the sphere

An element $u_t(i, j, k)$ of this matrix is the tangential velocity induced at the control point p_k, where the radial line towards the kth nascent vortex intersects the surface of the sphere by the ring vortex of unit strength at the grid (i, j), as shown in Figure 7.

5.5. Determination of the strengths of the nascent vortices

These strengths are determined so that the no-slip condition is satisfied on the surface of the sphere. More specifically, if the tangential velocity at the kth control point on the surface of the sphere is u_{tk}, which is composed of the tangential velocity due to the free stream and that induced by the ring vortices on all the nodes, the strength of the kth nascent vortex will be

$$\Gamma_k = u_{tk} r_{nsc} \Delta\theta, \tag{17}$$

with

$$u_{tk} = -\tfrac{3}{2} \sin\theta_k + \sum_{i=-M_N}^{M_P} \sum_{j=1}^{N_P} \Gamma(i, j)\, u_t(i, j, k). \tag{18}$$

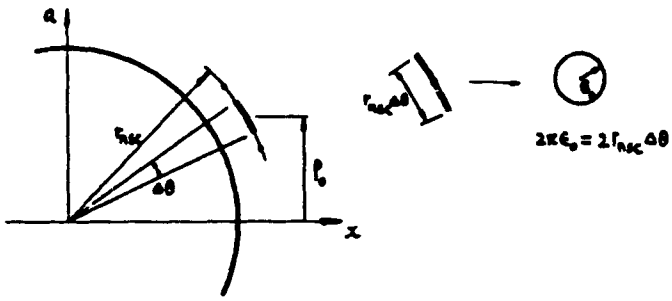

Figure 6. The core radius of a nascent vortex

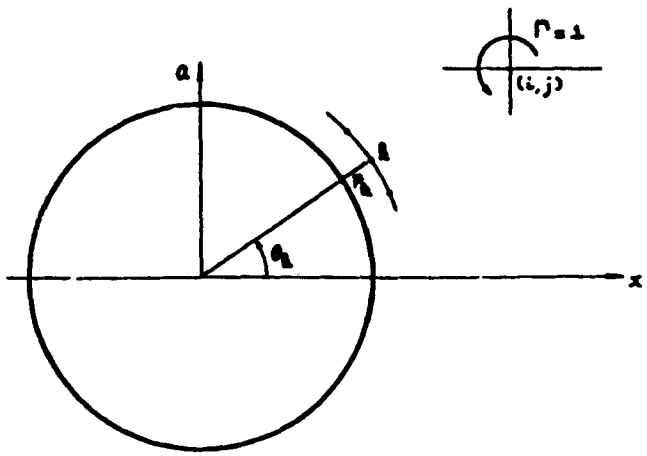

Figure 7. A control point on the surface of the sphere and a grid with a vortex of unit strength

The image vortices corresponding to these nascent vortices are also calculated, as equations (3) and (4) show, at this stage.

5.6. Transfer of the strengths of the nascent vortices and those of their images to the nodes

This is carried out according to the bivariate linear redistribution scheme as usual in the vortex-in-cell technique.[5,6]

5.7. Calculation of the velocity at the nodes of the mesh

The velocity components are calculated, by the use of the influence coefficients, from

$$u_{i,j}=u(x_i, a_j)=1+\frac{a_j^2-2x_i^2}{2r_{ij}^5}+\sum_{m=-M_N}^{M_P}\sum_{n=1}^{N_P}\Gamma(m,n)\,G_x(x_i, a_j; x_m, a_n), \tag{19a}$$

$$v_{i,j}=v(x_i, a_j)=-\frac{3a_jx_i}{2r_{ij}^5}+\sum_{m=-M_N}^{M_P}\sum_{n=1}^{N_P}\Gamma(m,n)\,G_a(x_i, a_j; x_m, a_n), \tag{19b}$$

where

$$r_{ij}=(x_i^2+a_j^2)^{1/2}. \tag{20}$$

It is only necessary to calculate the velocity at the 'active nodes', i.e. at the nodes of cells occupied by discrete vortex rings.

5.8. The velocity of each of the circular line vortices

The part of the velocity of a collective nature induced on each vortex may be reproduced from the velocity distribution, determined at the grid points at stage 5.7, by the usual technique of bivariate four-point interpolation. The self-induced velocity calculated by the use of equation (13) is added to this part to give the total velocity.

5.9. The new positions of the vortices

The positions of the discrete vortices are updated at each time step by a simple first-order integration scheme:

$$x_{k,\,\mathrm{new}}=x_{k,\,\mathrm{old}}+u_k\Delta t, \tag{21a}$$

$$a_{k,\,\mathrm{new}}=a_{k,\,\mathrm{old}}+v_k\Delta t. \tag{21b}$$

If desired, the computation can be terminated at this stage.

5.10. Calculation of the strengths and positions of the image vortices corresponding to this new distribution of vortices by the use of equations (3) and (4)

5.11. Transfer of the strengths of the vortices and those of their images to the relevant nodes of the mesh

The computation is repeated from stage 5.5 again.

6. COMPUTED RESULTS

It was found in the case of two-dimensional discrete vortex methods that the wake characteristics, and hence the forces experienced by the body, were dependent upon a non-dimensional

parameter made up of U, Δt and a length scale characterizing the model 'boundary layer thickness' at separation a_s, and also upon the ratio a_s/R. In the present instance a_s can be taken as proportional to $r_{nsc}-R$, and the appropriate parameter a_s^* as $(r_{nsc}-R)/U\Delta t$. In the case of two-dimensional flow it was found[16, 17] that provided that a_s^* lay within a narrow and well-defined range, realistic results were obtained for both flow patterns and forces. Furthermore, it was noted that when the flow patterns were realistic, the forces were generally well predicted by the models.

A parametric study was undertaken with the present model to determine values of a_s^* and a_s/R which produced flow patterns that resembled flow visualization photographs such as the one shown in Figure 1. Thirty-five vortex rings around the sphere were chosen as a standard, since this was found to be a sufficient number to satisfy the mean no-slip boundary condition. Calculation showed the tangential surface velocity to have an alternating sign of small amplitude. The amplitude diminished with increasing number of rings and was considered to be sufficiently small with 35 of them.

The results for $a_s^*=0{\cdot}4$ and $a_s/R=0{\cdot}08$ are shown in Figure 8. Of the cases investigated, this was considered to be the most realistic set of flow patterns. Another set, for comparison, is shown in Figure 9, with $a_s^*=0{\cdot}8$ and $a_s/R=0{\cdot}08$. In the two-dimensional case forces are conveniently calculated using the Blasius equation, which does not generalize to three dimensions since it is couched in terms of the theory of complex variables. For this reason forces and vortex-shedding frequencies were not calculated, although in principle the former could be by evaluating the pressure on the surface and integrating over the sphere, since the complex potential is known everywhere in the flow. Vortex-shedding frequencies are normally evaluated from force traces. They could also be estimated from the flow patterns, but this line was not pursued because the authors had no access to experimental data with which to compare them.

7. DISCUSSION OF RESULTS

It is well known that the wake behind a sphere shows different structures depending on the Reynolds number[7] and whether or not the flow is fully developed. For starting flows axisymmetric conditions exist. For the appropriate Reynolds number range the wake displays fluctuating shear layers, i.e. nodes of accumulated vorticity,[8] although they are neither as characteristically displayed nor as persistent as in a two-dimensional problem. Only a few nodes are clearly observable in a short distance downstream of the separation point. Beyond this distance the axisymmetry itself is not maintained.

The flow visualization photograph of Figure 1 shows a flow regime in which axisymmetric conditions exist in the near wake at a relatively high Reynolds number. The flow patterns shown in Figure 8 are qualitatively very similar to the photograph, although axisymmetry is maintained much further downstream than occurs for the real flow. It may be seen in the flow patterns that the separating shear layer forms circular nodes of concentrated vorticity that are carried downstream at regular intervals. The fact that only the second of the two models was able to predict such a flow suggests that the generation of countervorticity on the rear face of the sphere may well be an important factor in maintaining axisymmetric conditions in real flows too.

It must be emphasized that it is not being claimed that a flow pattern comparable with the observed one has been or can be produced, since it would be obviously futile to look for a 'model pattern' in a real unsteady flow. Why the method tends to produce a result simulating the flow of a particular range of Reynolds numbers is an intriguing question to which no clear answer can be offered except that it seems to be connected with the intrinsic property of vortices. Probably the answer should be sought from the relative importance of convection and velocity induced by vortices whose lateral range of distribution depends on the Reynolds number.

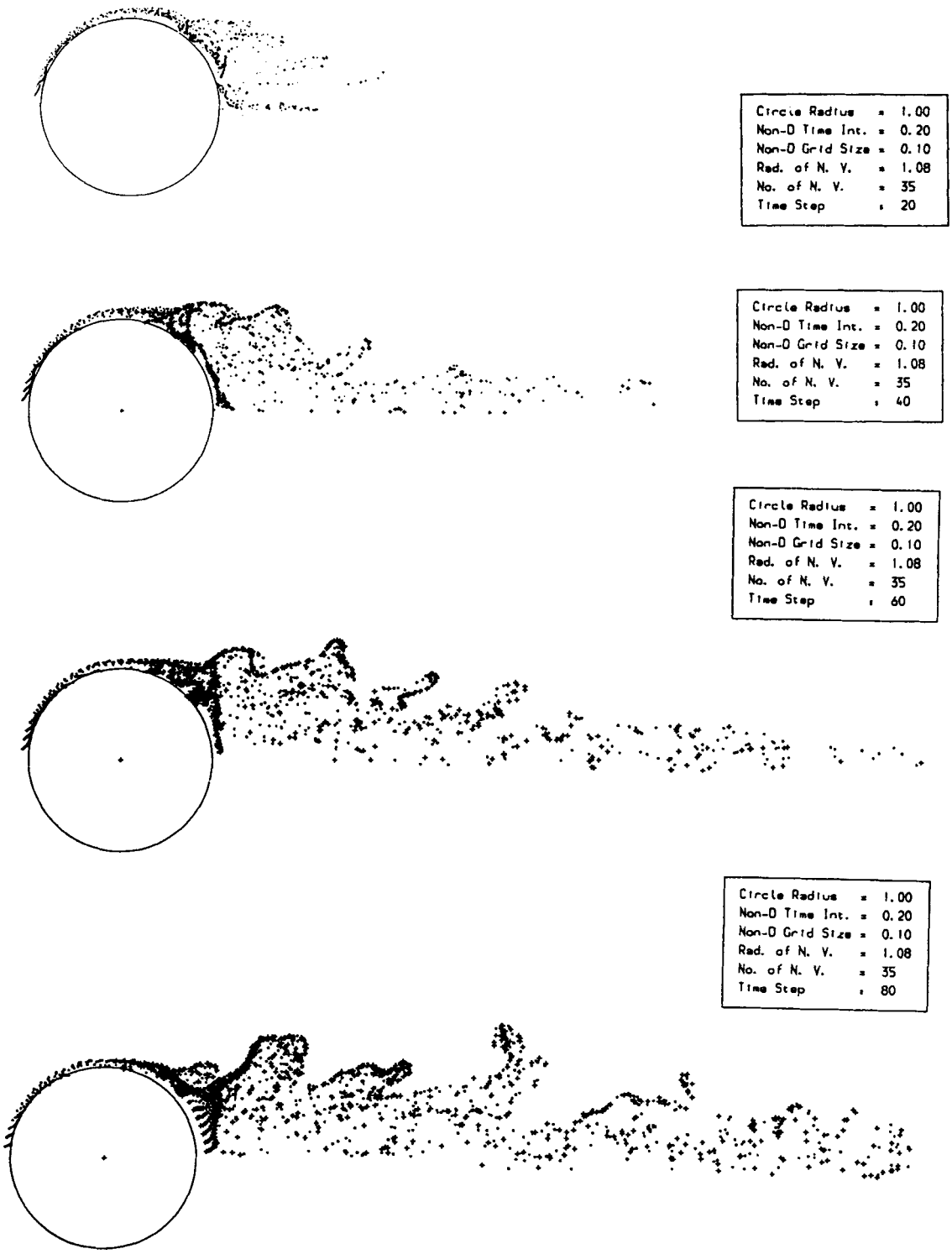

Figure 8. Flow patterns with $a_s^* = 0{\cdot}4$ and $a_s/R = 0{\cdot}08$

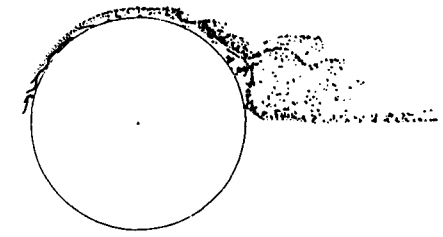

Circle Radius	=	1.00
Non-D Time Int.	=	0.10
Non-D Grid Size	=	0.10
Rad. of N. V.	=	1.08
No. of N. V.	=	35
Time Step	=	40

Circle Radius	=	1.00
Non-D Time Int.	=	0.10
Non-D Grid Size	=	0.10
Rad. of N. V.	=	1.08
No. of N. V.	=	35
Time Step	=	80

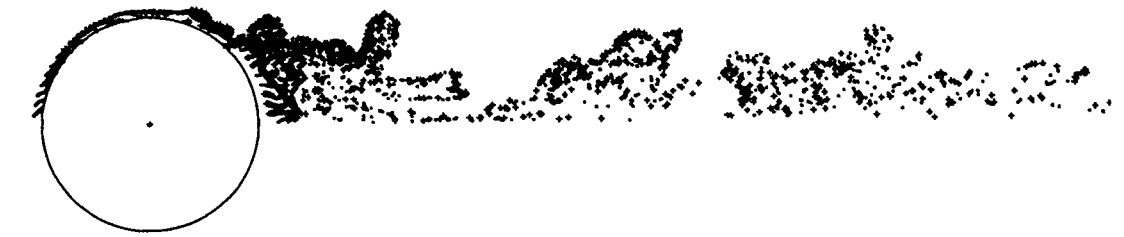

Circle Radius	=	1.00
Non-D Time Int.	=	0.10
Non-D Grid Size	=	0.10
Rad. of N. V.	=	1.08
No. of N. V.	=	35
Time Step	=	120

Figure 9. Flow patterns with $a_s^* = 0{\cdot}8$ and $a_s/R = 0{\cdot}08$

Breakdown of symmetry in reality is an aspect of flow which can hardly be coped with by the present discrete vortex method. Other three-dimensional versions of the technique, e.g. the vortex stick method or the vortex blob method, are under development to deal with a genuine three-dimensional problem, but not without sacrifice of the fundamental stipulation of the solenoidal property of the vorticity vector. This aspect alone, among others, can restrict the applicability of the method to simulate real flows.

8. CONCLUDING REMARKS

It has been demonstrated that the present model is viable from a computational point of view. It is strictly only applicable to starting flows about spheres, but it may well give interesting insights into the underlying mechanisms of other flows. It appears to reproduce some of the characteristics of the near wake of a more fully developed flow and suggests that the generation of counter-vorticity on the rear face of the sphere may well be an important mechanism for such flows. Finally, it could be used with some degree of confidence as the basis of a model for a truly axisymmetric flow existing at high Reynolds number.

ACKNOWLEDGEMENTS

The principal author has spent a year as Visiting Professor at the Department of Marine Technology, University of Newcastle upon Tyne. He would like to thank the Ministry of Education of the Korean Government and the Department of Marine Technology for making the visit possible.

APPENDIX: NOTATION

Γ	strength of a vortex
Γ_i	strength of an image vortex
U	far free stream velocity
u	component of velocity in axial direction
v	component of velocity in radial direction
ε	core radius
ε_0	initial core radius
c_c	core radius coefficient
ξ	x-co-ordinate of a circular line vortex
ρ	radius of a circular line vortex
ρ_0	initial radius of a circular line vortex
u_{self}	self-induced velocity in x-direction
r_{nsc}	radius of the spherical shell on which the nascent vortices are put
Δt	non-dimensional time step

REFERENCES

1. F. H. Abernathy and R. E. Kronauer, 'Formation of vortex streets', *J. Fluid Mech.*, **13**, 1–20 (1961).
2. J. H. Gerrard, 'Computation of magnitude and frequency of lift on a circular cylinder', *Phil. Trans. R. Soc.*, **261**, 137 (1967).
3. D. J. Maull, 'Flow models using vortex dynamics—work in the United Kingdom', *AGARD Advisary Report No. 239*, 1986.
4. T. Sarpkaya, 'Computational methods with vortices—The 1988 Freeman Lecture', *Trans. ASME, J. Fluids Eng.*, **111**, 5–52 (1989).

5. A. Leonard, 'Simulation of three-dimensional separated flows with vortex filaments', *Lecture Notes in Physics 59*, Springer, Berlin, 1976, pp. 280–284.
6. K. Kamemoto, K. Moriwaki and M. Aizawa, 'Numerical simulation of the axisymmetric vortex shedding from a ring by a discrete vortex method combined with the boundary element method', *Proc. Int. Sem. on Engineering Applications of the Surface and Cloud Vorticity Method, Pt. 2*, Technical University of Wroclaw, Wroclaw, 1987, pp. 33–43.
7. S. Taneda, 'Visual observations of the flow past a sphere at Reynolds numbers between 10^4 and 10^6', *J. Fluid Mech.*, **85**, pt. 1, 187–192 (1978).
8. H. Werlé, 'Principaux types de decollement libre observes sur maquettes ellipsoidales', *ONERA Report*, 1985.
9. G. K. Batchelor, '*An Introduction to Fluid Dynamics*', Cambridge University Press, Cambridge, 1967.
10. T. C. Lewis, 'On the images of vortices in a spherical vessel', *Q. J. Math.*, **XVI**, 338–347 (1879).
11. S. F. J. Butler, 'A note on Stokes's stream function for motion with a spherical boundary', *Proc. Camb. Phil. Soc.*, **49**, 169–174 (1953).
12. P. G. Saffman, 'The velocity of viscous vortex rings', *Stud. Appl. Math.*, **XLIX**, 371–380 (1970).
13. F. R. Hama, 'Progressive deformation of a curved vortex filament by its own induction', *Phys. Fluids*, **5**, 1156–1162 (1962).
14. J. P. Christiansen, 'Numerical simulation of hydrodynamics by the method of point vortices', *J. Comput. Phys.*, **13**, 363–379 (1973).
15. R. I. Lewis, *Vortex Element Methods for Fluid Flow Analysis*, Cambridge University Press, Cambridge, 1991.
16. K. Kamemoto and P. W. Bearman, 'The importance of timestep size and initial vortex position in the modelling of flows with discrete vortices', *IC Aero. Note 78-108*, Imperial College, London, 1978.
17. M. J. Downie, B. A. Murray and P. Bettess, 'Calculation of the force coefficients of a tubular jacket structural member with an appurtenance by the discrete vortex method', *Int. j. numer. methods eng.*, **27**, 153–167 (1989).